Exploring the selectivity of inhibitor complexes with Bcl-2 and Bcl-XL: A molecular dynamics simulation approach

Naoki Wakui [a],[1], Ryunosuke Yoshino [b],[c],[1], Nobuaki Yasuo [a], Masahito Ohue [a],[c], Masakazu Sekijima [a],[b],[c],[*]

[a] Department of Computer Science, School of Computing, Tokyo Institute of Technology, 2-12-1 Ookayama, Meguro-ku, Tokyo 152-8550, Japan
[b] Education Academy of Computational Life Sciences, Tokyo Institute of Technology, 4259 Nagatsutacho, Midori-ku, Yokohama, Kanagawa 226-8501, Japan
[c] Advanced Computational Drug Discovery Unit (ACDD), Institute of Innovative Research, Tokyo Institute of Technology, 4259 Nagatsutacho, Midori-ku, Yokohama, Kanagawa 226-8501, Japan

ARTICLE INFO

ABSTRACT

B-cell lymphoma 2 (Bcl-2) family proteins are potential drug targets in cancer and have a relatively flat and flexible binding site. ABT-199 is one of the most promising selective Bcl-2 inhibitors, and A-1155463 selectively inhibits Bcl-XL. Although the amino acid sequences of the binding sites of these two inhibitors are similar, the inhibitors selectively bind the target protein. In order to determine the origin of the selectivity of these inhibitors, we conducted molecular dynamics simulations using protein-inhibitor modeling. We confirmed that ASP103 of Bcl-2 is a key residue and that hydrogen bonding between ASP103 and ABT-199 confers the Bcl-2 selectivity of this inhibitor. For Bcl-XL selectivity, the secondary structure of α-helix 3 is a key factor. PHE105, SER106, and LEU108 in the loose α-helix 3 interact with A-1155463 to confer Bcl-XL selectivity. These findings provide important insights into the molecular mechanisms of selective inhibitors of Bcl-2 family proteins.

1. Introduction

Drug development is an expensive, time-consuming process; the cost is estimated to be approximately $2.6 billion dollars, and 12–14 years are required for a drug to reach the market [1]. To decrease these costs, computational techniques have been applied in various drug development studies, and many studies have successfully discovered new therapeutic compounds by employing computational techniques [2–5].

In drug discovery, computational methods are classified as structure-based drug discovery (SBDD) [6] or ligand-based drug discovery (LBDD) [7,8]. The SBDD method generally requires target structure information, such as X-ray structure data. In contrast, the LBDD method requires ligand structure information with experimental results. Molecular dynamics (MD) simulation, which can capture the intracellular dynamics of biomolecules at atomic-scale resolution, is a powerful computational tool for investigating protein-inhibitor interactions in SBDD. This simulation accounts for protein flexibility using Newtonian principles and has been applied to various biomolecules, such as nucleic acids, biomembranes, and proteins [9–18]. Recent studies have shown that MD simulations can be used to investigate the molecular mechanisms of the associations of inhibitors and proteins [19–22]. Physicochemical knowledge obtained from MD simulations can be broadly utilized for computational drug design [23] and can strongly support searches for seed compounds or acquisition of lead compounds in drug discovery.
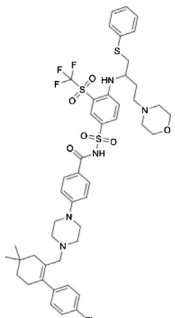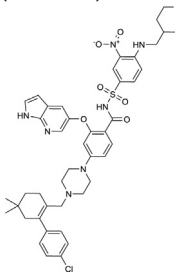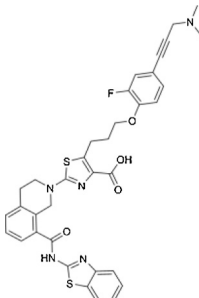
B-cell lymphoma 2 (Bcl-2) family proteins regulate programed cell death and are promising drug targets in cancer therapy [24,25]. To date, researchers have identified multiple anti-apoptotic Bcl-2 proteins, including Bcl-2, Bcl-XL, Bcl-w, Bcl2A1, and Mcl-1, and selective inhibitors have been developed for each of these proteins [26–32]. Bcl-2 family proteins share homologous sequences, e.g., the sequence identity between Bcl-2 and Bcl-XL is 50% (see sequence alignment in Fig. S1). Since the amino acid sequences of these proteins are very similar, the three-dimensional structures of both proteins are also similar, implying that inhibitors that can bind to Bcl-2 may also bind to Bcl-XL. Selectivity is one of the most

Table 1
Bcl-2 family protein inhibitors and protein-inhibitor complex structure information.

Compound	Bcl-2		Bcl-XL	
	Affinity K_d or K_i (nM)	Structure information (PDB ID)	Affinity K_d or K_i (nM)	Structure information (PDB ID)
ABT-263 (Navitoclax)	<0.044 [36]	4LVT [36]	<0.055 [36]	–
ABT-199	<0.010 [36]	–	48 [36]	–
A-1155463	80 [37]	–	<0.01 [37]	4QVX [37]

important factors affecting side effects in drug design [33,34], and it is extremely difficult to obtain selectivity in proteins belonging to the same family and having high sequence similarity [35]. ABT-263 (Navitoclax) [36] is an orally bioavailable small molecule that binds to both Bcl-2 and Bcl-XL. In preclinical studies, Navitoclax exhibited antitumor activity in lymphoid malignancies; however, thrombocytopenia was observed as the predominant side effect of Navitoclax when administered as single agent [37,38]. This was thought to be because lymphoid malignancies likely depend on Bcl-2 for survival and platelet survival depends on Bcl-XL [39,40]. Therefore, these observations prompted the idea that selective inhibition of a single Bcl-2 family protein has promising potential in targeting specific cancer types.

ABT-199 [41] and A-1155463 [42] are Bcl-2-selective and Bcl-XL-selective inhibitors, respectively. ABT-737 [43] and ABT-263 (Navitoclax) [36] bind to both Bcl-2 and Bcl-XL, and complex structures of Bcl-XL/ABT-737 [44] and Bcl-2/ABT-263 [41] have been determined by X-ray crystallography. In addition, the complex structures of Bcl-XL/WEHI-539 [30] and Bcl-XL/Compound 10 [45] have also been determined. However, the structures of Bcl-2/ABT-199, Bcl-2/A-1155463, Bcl-2/WEHI-539, Bcl-2/compound 10, Bcl-XL/ABT-199, and Bcl-XL/ABT-263 have not been determined

yet (Table 1). Although this structural information is indispensable for elucidating the mechanism of inhibition, information obtained from crystal structures is limited, and further information is needed to clarify the dynamics of proteins or protein-inhibitor interactions in complexes. MD simulations, which can be used to observe dynamic behaviors of biomolecules, are necessary to investigate not only the snapshot of stable interactions, but also the dynamic interactions between residues and atoms of inhibitors and to discover the origin of selectivity. Furthermore, only complex structures of proteins to which their selective inhibitors bind can be obtained, and complex structures of proteins to which nonselective inhibitors bind cannot be obtained or can be quite difficult to obtain.

Protein-ligand complex modeling is a computational technique in which virtual/theoretical complex structures of the protein and desired compound are generated. This method is widely used in computer-aided drug design and is highly compatible with MD simulation. Accordingly, in this study, we performed computational protein-inhibitor complex modeling and MD simulation for each complex structure to elucidate factors affecting selectivity. We report the results of MD simulation of either ABT-199 or A-1155463 complexed with Bcl-2 and Bcl-XL and show structural consider-
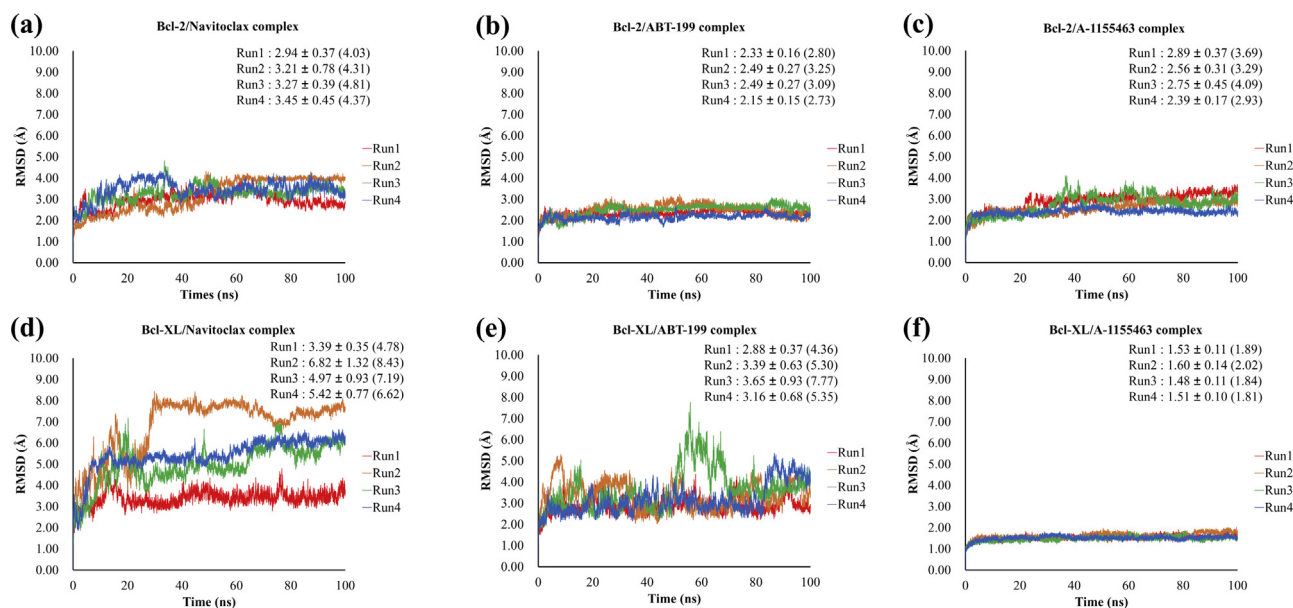
Fig. 1. Comparison of the RMSD time courses of all complexes. The mean and max RMSD values were calculated for each complex, and the maximum values are shown in parentheses. (a) Bcl-2/Navitoclax complex. (b) Bcl-2/ABT-199 complex. (c) Bcl-2/A-1155463 complex. (d) Bcl-XL/Navitoclax complex. (e) Bcl-XL/ABT-199 complex. (f) Bcl-XL/ABT-199 complex. (f) Bcl-XL/A-1155463 complex.

Table 2

Summary of residues that interacted, include water-bridged hydrogen bond, more than averagely 30% of the simulation time. Average interaction rate and standard deviation are shown in parentheses.

Compound	Bcl-2	Bcl-XL
Navitoclax	TYR108 (60.9 ± 7.7%)	ARG100 (31.2 ± 8.2%),
	MET115 (53.7 ± 6.5%),	TYR101 (48.9 ± 10.5%)
	LEU137 (31.0 ± 1.8%),	
	ASN143 (60.9 ± 7.7%),	
	TYR202 (81.9 ± 8.7%)	
ABT-199	ASP103 (97.7 ± 1.5%),	GLU96 (41.8 ± 19.9%),
	PHE104 (30.8 ± 2.3),	PHE97 (39.9 ± 6.7%),
	TYR108 (69.2 ± 11.6%),	TYR101 (78.1 ± 5.71%),
	MET115 (41.5 ± 5.5%),	LEU108 (38.5 ± 4.9%),
	ASN143 (62.8 ± 7.5%),	ASN136 (51.8 ± 7.7%),
	TYR202 (86.2 ± 3.6%)	TYR195 (80.7 ± 4.6%)
A-1155463	ASP103 (44.3 ± 19.9),	TYR101 (52.5 ± 9.2%),
	PHE104 (36.9 ± 7.8%),	PHE105 (73.8 ± 4.7),
	PHE112 (41.8 ± 4.0%),	SER106 (58.8 ± 6.7%),
	LEU137 (37.9 ± 4.5%),	LEU108 (53.3 ± 9.8%),
	ASN143 (32.7 ± 7.6),	LEU130 (56.1 ± 15.3%),
	ARG146 (53.2 ± 5.1%),	ASN136 (36.4 ± 10.7%),
	TYR202 (38.2 ± 9.7%)	ARG139 (53.5 ± 9.3%),
		ALA149 (43.1 ± 3.3%)

ations of the factors affecting the selectivity of Bcl-2 and Bcl-XL inhibitors.

2. Materials and methods

2.1. Preparation of the protein structures for MD simulation

The X-ray structures of Bcl-2/Navitoclax complex (PDB ID: 4LVT) and Bcl-XL/A-1155463 complex (PDB ID: 4QVX) were taken from the Protein Data Bank (PDB) [46]. The structures were subjected to assignment of bond orders, hydrogenation, and creation of zero-order bonds to metal and disulfide bonds. The suitable ionization states of bound inhibitors were generated at pH 7.0 ± 2.0 with Epik [47] (Fig. S2 and Table S1). H-bond optimization was performed with protonation states of residues at pH 7.0 as determined from a pKa prediction using PROPKA [48]. Thereby, the removal

of unwanted water molecules and optimization of energy were conducted with Maestro using the OPLS3 force field [43].

To build four protein/inhibitor complexes (Bcl-2/ABT-199, Bcl-2/A-1155463, Bcl-XL/ABT-199, and Bcl-XL/Navitoclax), the X-ray structures of Bcl-2/Navitoclax analog complex (PDB ID: 4MAN), Bcl-2/Navitoclax complex (PDB ID: 4LVT), Bcl-XL/A-1155463 complex (PDB ID: 4QVX), and Bcl-XL/HBx-BH3 motif complex (PDB ID: 5B1Z) were taken from the PDB because the Navitoclax analog in 4MAN is structurally the most similar to ABT-199 (Tanimoto similarity: 0.908) and Bcl-XL/HBx-BH3 motif complex (PDB ID: 5B1Z) is similar to Bcl-2/Navitoclax complex (PDB ID: 4LVT) and Bcl-2/Navitoclax analog complex (PDB ID: 4MAN). To build the Bcl-2/ABT-199 complex, 4MAN was used. We converted the Navitoclax analog to ABT-199 using "3D Builder" in Maestro (Schrödinger, LLC). To build the Bcl-2/A-1155463 complex, 4MAN and 4QVX were used. Protein structure alignment of 4MAN and 4QVX based on protein alpha carbon (Cα) was performed with Maestro because protein-ligand docking simulation failed to obtain the desired complex structure because of ligand flexibility. The structures of Navitoclax analog and Bcl-XL protein were deleted and the structures of Bcl-2 and A-1155463 were merged. To build the Bcl-XL/ABT-199 complex and Bcl-XL/Navitoclax complex, 5B1Z and Bcl-2/ABT-199 complex and 5B1Z and 4LVT were used, respectively. Protein structure alignments and deletions of unnecessary structures were conducted as described above. The four structures were also subjected to assignment of bond orders, hydrogenation, creation of zero-order bonds to metal and disulfide bonds, generation of suitable ionization state, and H-bond optimization, thereby removing water molecules and optimizing energy with Maestro using the OPLS3 force field.

2.2. Preprocessing for MD simulations

Molecular Dynamics System Setup Module [50] was used to set up systems. The protein-inhibitor complex was immersed in the orthorhombic box with a buffer distance of 10 Å using the simple point charge (SPC) water model. The systems were neutralized by adding counterions and 0.15 M NaCl. Box size and the total number of atoms of each system are summarized in Table S2 and the set-up systems are shown in Fig. S3.
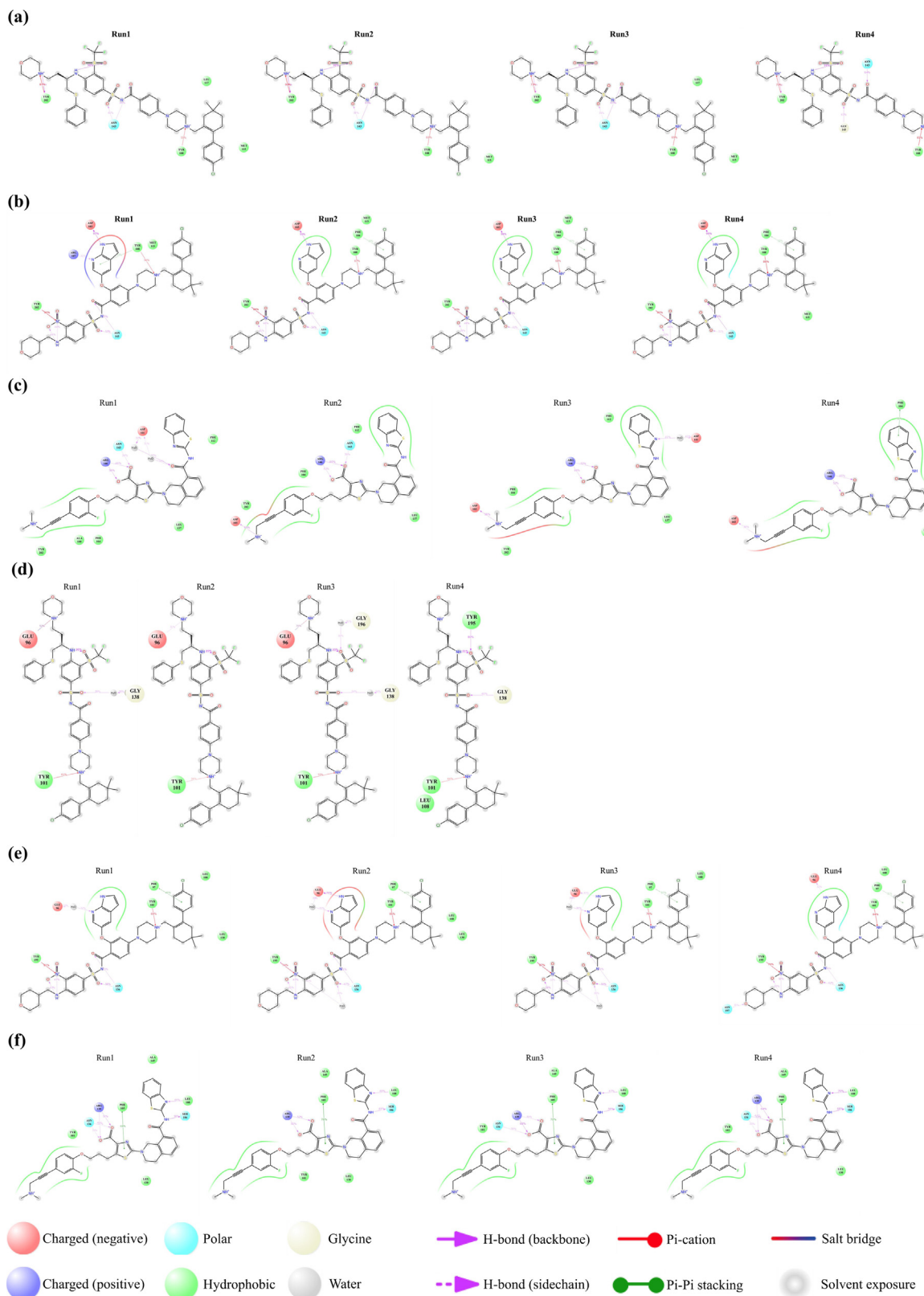
Fig. 2. 2D summary views of the protein-inhibitor interactions. Residues that interacted for more than 30% of the simulation time are indicated. H-bond (backbone, sidechain), π-π stacking, π-cation, and salt bridge are shown by their symbols as displayed in the key. (a) Interactions between Bcl-2 and Navitoclax. (b) Interactions between Bcl-2 and ABT-199. (c) Interactions between Bcl-2 and A-1155463. (d) Interactions between Bcl-XL and Navitoclax. (e) Interactions between Bcl-XL and ABT-199. (f) Interactions between Bcl-XL and A-1155463.
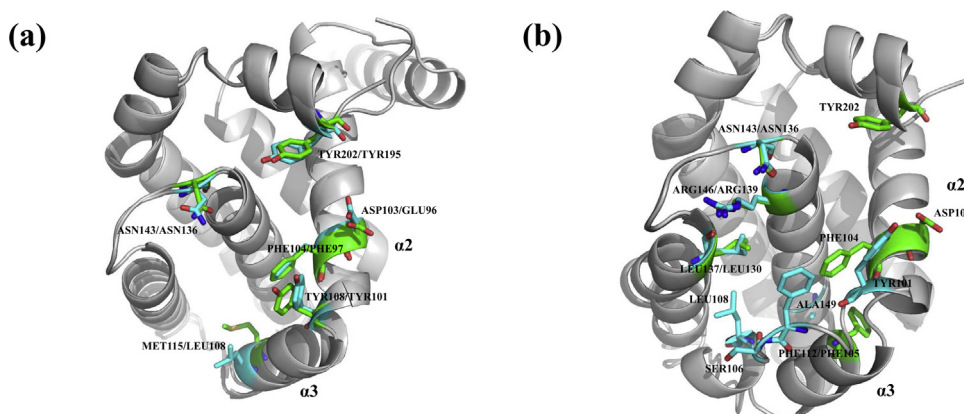
Fig. 3. Summary of interaction comparisons. (a) Structural alignment of ABT-199 bound to Bcl-2 and Bcl-XL. Residues that interacted more than 30% of the simulation time are represented as stick models and colored green in Bcl-2 or cyan in Bcl-XL. (b) Structural alignment of A-1155463 bound to Bcl-2 and Bcl-XL. Residues that interacted more than 30% of the simulation time are represented as stick models and colored green in Bcl-2 or cyan in Bcl-XL. (For interpretation of the references to colour in this figure legend, the reader is referred to the web version of this article.)
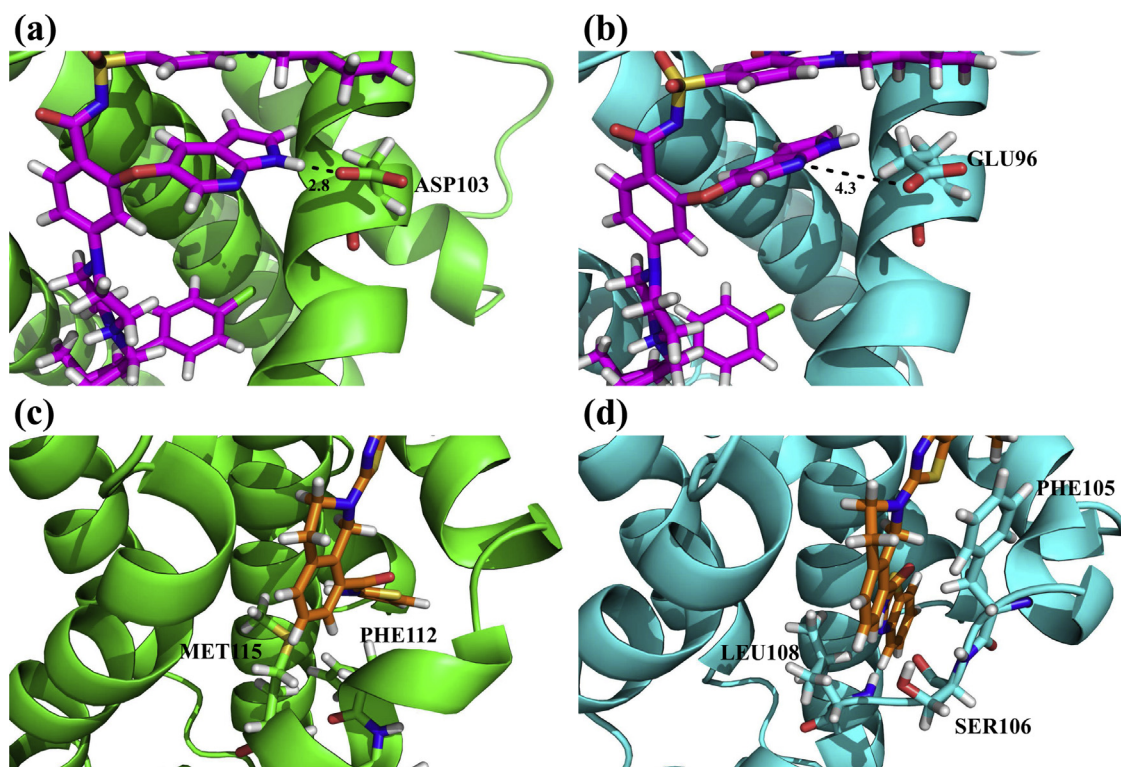

Fig. 4. Key interactions of ABT-199 and A-1155463, as observed in representative structures of the most populated structural clusters in each MD simulation. Bcl-2 (green) and Bcl-XL (cyan) are represented as cartoon models, and ABT-199 (magenta) and A-1155463 (orange) are represented as stick models. Nitrogen, oxygen, sulfur, and chloride atoms are colored blue, red, yellow, and green, respectively. (a) Interaction between ASP103 of Bcl-2 and ABT-199. (b) Interaction between GLU96 of Bcl-XL and ABT-199. (c) Interaction between Bcl-2 and A-1155463. (d) Interaction between Bcl-XL and A-1155463. Key residues (PHE105, SER106, and LEU108) are represented as a stick model. (For interpretation of the references to colour in this figure legend, the reader is referred to the web version of this article.)

2.3. MD simulations

The Desmond MD package [50] was used for all constructed systems. The OPLS3 force field [49] was used to calculate the interactions between all atoms. The "u-series" algorithm developed at D.E. Shaw Research [51] was used for calculating the long-range Coulombic interactions. The cut-off radius was set to 9 Å for the short-range van der Waals and electrostatic interactions. Initial temperature and pressure were set to 300 K and 1.01325 bar, respectively. Temperature and pressure were controlled during the simulations using the Nose-Hoover thermostat [52,53] and the Martyna-Tobias-Klein method [54], respectively. A time step of 2.0 fs was used for the simulations. The default protocols of the Desmond package were used for minimization and MD equilibration of the systems. Finally, 100-ns atomistic MD simulations for each protein-inhibitor complex system were performed four times by changing the initial seed, and the collected trajectory frames throughout the MD simulations were used in the post-processing MD analysis. Spacing information for the "u-series" algorithm and initial seeds are summarized in Table S2.

2.4. Post-processing MD analysis

The trajectory frames, obtained from the MD simulations, were subjected to post-processing MD analysis to quantitatively measure the protein-inhibitor interactions. The protocols implemented

in the Maestro small-molecule drug discovery suite were used to define hydrogen bonds, hydrophobic interactions, π-π stacking, and salt-bridge interactions.

2.5. Trajectory clustering analysis

The Desmond trajectory clustering tool was used to select representative structures from the simulations. The heavy-atom root mean square deviation (RMSD) matrix was used as a structural similarity metric, and hierarchical clustering with average linkage was used as the clustering method. The merging distance cutoff was set to be 2.0 Å. The structure with the largest number of neighbors in the structural family was used as the representative structure.

3. Results

The four modeled protein/inhibitor complexes were proved to be well established in terms of interactions between protein and inhibitor (details are described in the Supplementary Materials), and the following analyses were conducted based on these structures.

3.1. Structural stability analysis

RMSD values of the heavy atoms referenced with the initial structure were calculated for each complex. The time course of RMSD for each complex during the 100-ns MD simulations is shown in Fig. 1. The RMSD of all simulation systems approached stable values in the final 30 ns. This indicated that the six protein/inhibitor complexes had been equilibrated, enabling the following analysis. The highest average RMSD value among the six protein-inhibitor complexes was observed for the Bcl-XL/Navitoclax complex, and ranged from 3.39 to 6.82 Å. This is because the N-terminal of α-helix 1 showed high fluctuation (Fig. S5). For the Bcl-2/ABT-199 and Bcl-XL/ABT-199 complexes, the average RMSD values ranged from 2.15 to 2.49 Å and from 2.88 to 3.65 Å, respectively (Fig. 1b,e). The region of the Bcl-XL/ABT-199 complex that showed the highest fluctuation was the N-terminal of α-helix 1 (Fig. S5). Although both complex structures were modeled structures, this result suggested that the Bcl-2/ABT-199 complex was more stable than the Bcl-XL/ABT-199 complex. For the Bcl-2/A-1155463 and Bcl-XL/A-1155463 complexes, the average RMSD values ranged from 2.39 to 2.89 Å and from 1.48 to 1.60 Å, respectively (Fig. 1c,f). The Bcl-XL/A-1155463 complex was the most stable complex among the four complexes.

3.2. Protein-inhibitor interaction analysis

To analyze the interactions between proteins and inhibitors, interaction analysis was carried out for the six protein/inhibitor complexes.

3.2.1. Bcl-2/Navitoclax complex

There were 28 residues that interacted with Navitoclax (Fig. S6a), and five residues interacted more than 30% of the simulation time, on average (Fig. 2a, Table 2 and Table S3). TYR108 formed a π-cation interaction with the nitrogen atom of piperazine. MET115 and LEU137 exhibited a hydrophobic interaction around the P2 pocket. ASN143 formed a hydrogen bond with either the oxygen atom of sulfone or that of amide from sulfonylbenzamide. TYR202 formed a π-cation interaction with the nitrogen atom of morpholine.

3.2.2. Bcl-2/ABT-199 complex

There were 23 residues that interacted with ABT-199 (Fig. S6b), and six residues interacted more than 30% of the simulation time,

on average (Fig. 2b, Table 2 and Table S4). ASP103 formed a hydrogen bond with the nitrogen atom of azaindole. PHE104 formed π-π stacking interactions with chlorophenyl. TYR108 formed either a π-cation interaction with the nitrogen atom of piperazine or a π-π stacking interaction with azaindole. MET115 exhibited a hydrophobic interaction, and ASN143 formed a hydrogen bond with either the oxygen atom of sulfone or that of amide from sulfonylbenzamide. TYR202 formed a π-cation interaction with the nitrophenyl.

3.2.3. Bcl-2/A-1155463 complex

There were 36 residues that interacted with A-1155463 (Fig. S6c), and seven residues interacted more than 30% of the simulation time, on average (Fig. 2c, Table 2, and Table S5). PHE112, LEU137, and TYR202 had hydrophobic interactions with A-1155463. ASP103 formed a hydrogen bond with the dimethylamino group. PHE104 had either hydrophobic interactions or π-π stacking interactions with benzothiazole. ASN143 and ARG146 formed hydrogen bonds with the oxygen atom of the amide from thiazole carboxylic acid.

3.2.4. Bcl-XL/Navitoclax complex

There were 39 residues that interacted with Navitoclax (Fig. S6d), and two residues interacted more than 30% of the simulation time, on average (Fig. 2d, Table 2 and Table S6). ARG100 showed an ionic interaction with the trifluoromethylsulfonyl phenyl group. TYR101 formed a π-cation interaction with the nitrogen atom of piperazine.

3.2.5. Bcl-XL/ABT-199 complex

There were 33 residues that interacted with ABT-199 (Fig. S6e), and six residues interacted more than 30% of the simulation time, on average (Fig. 2e, Table 2 and Table S7). GLU96 formed either water-bridged or direct hydrogen bonds with the nitrogen atom of azaindole. PHE97 formed π-π stacking interactions with chlorophenyl, and TYR101 formed a π-cation interaction with the nitrogen atom of piperazine. LEU108 had a hydrophobic interaction with ABT-199. ASN136 formed a hydrogen bond with either the oxygen atom of sulfone or that of amide from sulfonylbenzamide. TYR195 formed a π-cation interaction with the nitrophenyl group.

3.2.6. Bcl-XL/A-1155463 complex

There were 28 residues that interacted with A-1155463 (Fig. S6f), and eight residues interacted more than 30% of the simulation time, on average (Fig. 2f, Table 2 and Table S8). TYR101 exhibited hydrophobic interactions and PHE105 formed π-π stacking interactions with the thiazole ring. The backbone of SER106 and LEU108 formed hydrogen bonds with the nitrogen atom of the carbamoyl group and the nitrogen atom of the benzothiazole, respectively. LEU130, ASN136, and ARG139 showed the same interactions as those observed in the Bcl-2/A-1155463 complex. ALA149 had a hydrophobic interaction with the benzothiazole group.

3.3. Interaction comparison

3.3.1. Comparison of Bcl-2/Navitoclax complex and Bcl-XL/Navitoclax complex

Navitoclax is known to inhibit both Bcl-2 and Bcl-XL, and the binding affinities are comparable (Table 1). Interactions between Navitoclax and Bcl-2 or Bcl-XL could provide a standard for understanding selective inhibitors. TYR108 in Bcl-2 was found to correspond to TYR101 in Bcl-XL and showed similar interactions (Fig. 2a, d and Fig. S1). The remainder of the residues that interacted more than 30% of the simulation time, on average, also showed similar interactions, whereas the corresponding residues in the other complex interacted less than 30% of the simulation time. Given

the similar interaction between Navitoclax and Bcl-2 and Bcl-XL, Navitoclax can inhibit both proteins.

3.3.2. Comparison of Bcl-2/Navitoclax complex and Bcl-2/ABT-199 complex

As the basic design of ABT-199 was derived from Navitoclax, TYR108, MET115, ASN143, and TYR202 showed interactions similar to those seen in the Bcl-2/Navitoclax complex. The Bcl-2/ABT-199 complex had two additional interaction residues (ASP103 and PHE104). ASP103 interacted with the nitrogen atom of azaindole. PHE104 interacted with not only chlorophenyl but also azaindole in the Bcl-2/ABT-199 complex.

3.3.3. Comparison of Bcl-2/ABT-199 complex and Bcl-XL/ABT-199 complex

Comparison of the residues in the Bcl-2/ABT-199 and Bcl-XL/ABT-199 complexes that interacted more than 30% of the simulation time, on average showed that most of the interactions were similar in both complexes. The only differences were ASP103 in Bcl-2 and GLU96 in Bcl-XL, which were both acidic residues and were located at the same structural position. The distance between ASP103 and the nitrogen atom of azaindole was 2.8 Å in the representative structure of the most populated structural clusters (Fig. 4a), and ASP103 formed a direct hydrogen bond with the nitrogen atom of azaindole, whereas the distance between GLU96 and the nitrogen atom of the azaindole was 4.3 Å in the representative structure (Fig. 4b). This, together with the simulation interaction analysis (Fig. 2e, Fig. S6e), suggested that GLU96 forms water-bridged hydrogen bonds with azaindole at a higher frequency than ASP103.

3.3.4. Comparison of Bcl-XL/Navitoclax complex and Bcl-XL/A-1155463 complex

Interactions between Bcl-XL/Navitoclax and Bcl-XL/A-1155463 were totally different because they have different mother nuclei. The Bcl-XL/A-1155463 complex gained interactions with PHE105, SER106, LEU108, LEU130, ASN136, ARG139, and ALA149 (Table 2). Interestingly, TYR101 and LEU108 were involved in inhibitor interactions, but their interactions were different. TYR101 in the Bcl-XL/Navitoclax complex showed a π-cation interaction with piperazine, whereas TYR101 in the Bcl-XL/A-1155463 complex showed a hydrophobic interaction with the fluorophenoxy group. LEU108 in Bcl-XL/Navitoclax showed a hydrophobic interaction around the P2 hotspot, whereas LEU108 in Bcl-XL/A-1155464 formed a hydrogen bond using its backbone.

3.3.5. Comparison of the Bcl-2/A-1155463 complex and Bcl-XL/A-1155463 complex

Comparison of the residues in Bcl-2 and Bcl-XL that interacted more than 30% of the simulation time, on average, showed that LEU137, ASN143, and ARG146 in Bcl-2, corresponding to LEU130, ASN136, and ARG139 in Bcl-XL, were identical (Fig. 3b, Table 2 and Fig. S1); these residues interacted with A-1155463 in the same way. PHE112 in Bcl-2 and PHE105, SER106, and LEU108 in Bcl-XL were located in α-helix 3; however, their interactions were different. PHE112 showed a hydrophobic interaction around the P2 hotspot. SER106 and LEU108 formed hydrogen bonds with their backbones rather than their side chains. PHE105, which corresponded to PHE112 in Bcl-2, did not have a hydrophobic interaction around the P2 hotspot, but had a π-π interaction. In addition to LEU130, ALA149 in Bcl-XL also had a hydrophobic interaction around the P2 hotspot.

4. Discussion

4.1. Selectivity of the Bcl-2-selective inhibitor

There are a few amino acid differences within the BH3-binding site between Bcl-2 and Bcl-XL. The difference between ASP103 in Bcl-2 and GLU96 in Bcl-XL is considered to be a key factor affecting the Bcl-2 selectivity of the inhibitor [41]. We showed that there were differences in the interactions between ASP103 and ABT-199 and between GLU96 and ABT-199, even though the only difference between asparagine and glutamic acid is the number of carbon atoms. ASP103 formed a hydrogen bond with the nitrogen atom of azaindole, and its average retention time was $97.7 \pm 1.5\%$ (Fig. 2b and Table 2). In contrast, GLU96 formed a hydrogen bond, and the average retention time was $41.8 \pm 19.9\%$, or for a water-bridged hydrogen bond, the average retention time was $34.8 \pm 6.4\%$, with the nitrogen atom of azaindole (Fig. 2e, Table S7). In addition to the interaction analysis, we conducted a MM-GBSA calculation for the Bcl-2(D103E)/ABT-199 complex. $\Delta\Delta G_{bind}$ of Bcl-2/ABT-199 and Bcl-2(D103E)/ABT-199 was estimated to be 13.5 kcal/mol (Table S10). This result suggests that the binding energy of the D103E mutant Bcl-2/ABT-199 complex is unfavorable compared to that of the native Bcl-2/ABT-199 complex. In terms of energy, ASP103 affected the binding of ABT-199 and Bcl-2 selectivity. In the development of ABT-199, the indole was replaced with an azaindole as the P4-binding moiety, and azaindole was expected to be able to interact with ARG107 [41]. However, interaction between ARG107 and azaindole was hardly observed during MD simulation of the Bcl-2/ABT-199 complex. ARG107 was perfectly oriented to form hydrogen bonds and a salt bridge with ASP103, and these interactions were observed most of the simulation time (Fig. S7b). These interactions kept ASP103 facing the azaindole and stabilized the hydrogen bond. Although ARG100 in Bcl-XL also formed hydrogen bonds and a salt bridge with GLU96, GLU96 did not face the azaindole in each representative structure (Fig. S7d). The length of the carbon chain and interactions with ARG107/ARG100 resulted in interaction differences. We showed that azaindole was less likely than expected to interact with ARG107, and we thus suggest a replacement of azaindole with indole to enhance Bcl-2 selectivity. GLU96 tended to form a water-bridged hydrogen bond with the nitrogen atom of pyridine; thus, replacement of azaindole to indole might decrease the water-bridged hydrogen bonding between Bcl-XL and ABT-199. ΔG_{bind} of Bcl-2/ABT-199 (indole analog) was comparable to that of Bcl-2/ABT-199, and $\Delta\Delta G_{bind}$ of Bcl-2/ABT-199 (indole analog) and Bcl-XL/ABT-199 (indole analog) were much larger than those of Bcl-2/ABT-199 and Bcl-XL/ABT-199 (Table S10).

4.2. Selectivity of the Bcl-XL inhibitor

Based on the protein-inhibitor interaction analysis, most of the residues in Bcl-2 and Bcl-XL that interacted with A-1155463, a Bcl-XL selective inhibitor, were the same. Only PHE105, SER106, and LEU108, corresponding to PHE112, ALA113, and MET115 in BCL-2, were different (Fig. 2c and 2f). A comparison of the representative structures of Bcl-2 and Bcl-XL generated using the clustering method showed that the secondary structure of α-helix 3, in which PHE105, SER106, and LEU108 were located, was completely different (Fig. 4c and 4d). In Bcl-XL, substantial changes in the backbone conformation at α-helix 3 and α-helix 4 have been reported [55]. Unfolding of α-helix 3 in Bcl-XL is observed in apo and the Bak and Beclin-1 peptide-bound structures [56–58]; in contrast, when bound to Bim or ABT-737, α-helix 3 remains helical [59,44]. For Bcl-XL/A-1155463, α-helix 3 is unfolded and shows a loop structure in crystals [42] (Fig. S8), and this secondary structure was maintained during MD simulation. PHE105, SER106, and LEU108 gained interactions with A-1155463 because of the unfolding of α-helix

3. PHE105 of Bcl-XL and the thiazole ring formed π-π stacking interactions, whereas PHE112 of Bcl-2 constituted a P2 hotspot and showed hydrophobic interaction. PHE105 was outside of the P2 hotspot, making the P2 hotspot deeper and the hydrophobic groove narrower (Fig. S9). Moreover, the backbones of SER106 and LEU108 formed hydrogen bonds with the nitrogen atom of the carbamoyl group and the nitrogen atom of benzothiazole, respectively, and the importance of the hydrogen bonds was consistent with descriptors of QSAR models of benzothiazole derivatives [59]. As the backbones of ALA113 and MET115 were used for inter-residue hydrogen bonds to constitute the α-helix, their backbones could not form interactions with A-1155463. These crystal structures and MD simulations suggested that the backbone changed in the flexible α-helix 3 to expose a large hydrophobic groove, which was used in binding to inhibitors. Additionally, the secondary structure of the flexible α-helix 3 was found to be a key factor affecting the selectivity of Bcl-XL-selective inhibitors.

5. Conclusion

Understanding of protein-inhibitor interactions is important for designing target-selective inhibitors. In this study, we applied an approach that combined modeling and MD simulation to improve the current understanding of the selectivity of ABT-199 for Bcl-2 and A-1155463 for Bcl-XL. For Bcl-2-selective inhibitors, our study confirmed that the hydrogen bond between ASP103 of Bcl-2 and azaindole of ABT-199 was a key interaction as indicated by interaction analysis and MM-GBSA analysis, and we suggest that replacement of azaindole with indole can increase selectivity. For Bcl-XL-selective inhibitors, our study suggests that the secondary structure of the flexible α-helix 3, i.e., unfolding of α-helix 3 and exposure of PHE105, SER106, and LEU108 to the binding site, was essential. These residues formed a π-π interaction or hydrogen bonds with the Bcl-XL-selective inhibitor. Thus, selective inhibitors should be designed based on both differences in amino acid sequences and differences in the secondary structures of proteins.

Without X-ray structures, it is difficult to compare interactions between protein-inhibitor complexes of interest. Protein-inhibitor complex modeling, as applied in this study, at least enables comparison of interactions; however, it does not explain the selectivity. By combining MD simulation, interaction analysis, and clustering analysis, stable interactions between protein and inhibitor could be clarified. Therefore, MD simulation is a powerful tool for elucidating the dynamics of protein-inhibitor interactions and to support drug design. The insights obtained from the MD simulations may be useful for designing new selective Bcl-2 or Bcl-XL inhibitors.

Acknowledgments

Appendix A. Supplementary data

Supplementary data associated with this article can be found, in the online version, at https://doi.org/10.1016/j.jmgm.2017.11.011.

References

[1] S.P. Leelananda, S. Lindert, Computational methods in drug discovery, J. Org. Chem. 12 (2016) 2694–2718.
[2] R. Yoshino, N. Yasuo, D.K. Inaoka, Y. Hagiwara, K. Ohno, M. Orita, M. Inoue, T. Shiba, S. Harada, T. Honma, B.E. Oluwadae, R.J. Rodrigues, M.C. Alberto, K. Kita, M. Sekijima, Pharmacophore modeling for anti-Chagas drug design using the fragment molecular orbital method, PLoS One 10 (2015) e0125829.
[3] R. Yoshino, N. Yasuo, Y. Hagiwara, T. Ishida, D.K. Inaoka, Y. Amano, Y. Tateishi, K. Ohno, I. Namatame, T. Niimi, M. Orita, K. Kita, Y. Akiyama, M. Sekijima, *In silico*, *in vitro*, X-ray crystallography, and integrated strategies for discovering spermidine synthase inhibitors for Chagas disease, Sci. Rep. 7 (2017) 6666.
[4] S. Chiba, et al., Identification of potential inhibitors based on compound proposal contest: tyrosine-protein kinase Yes as a target, Sci. Rep. 5 (2015) 17209.
[5] S. Chiba, et al., An iterative compound screening contest method for identifying target protein inhibitors using the tyrosine-protein kinase Yes, Sci. Rep. 7 (2017) 12038.
[6] T. Kindt, et al., Structure-based strategies for drug design and discovery, Nature 352 (1991) 581.
[7] O.F. Güner (Ed.), Pharmacophore perception, development, and use in drug design, Vol. 2, International University Line, 2002.
[8] A. Tropsha, QSAR in drug discovery, Drug Des. Struct. Ligand-Based Appr. (2010) 151–164.
[9] K. Arora, C.L. Brooks, Functionally important conformations of the Met20 loop in dihydrofolate reductase are populated by rapid thermal fluctuations, J. Am. Chem. Soc. 131 (2009) 5642–5647.
[10] J.I. Sulkowska, J.K. Noel, J.N. Onuchic, Energy landscape of knotted protein folding, Proc. Natl. Acad. Sci. U. S. A. 109 (2012) 17783–17788.
[11] K. Nam, J.Z. Pu, M. Karplus, Trapping the ATP binding state leads to a detailed understanding of the F1-ATPase mechanism, Proc. Natl. Acad. Sci. U. S. A. 111 (2014) 17851–17856.
[12] R.L. Hayes, J.K. Noel, U. Mohanty, P.C. Whitford, S.P. Hennelly, J.N. Onuchic, K.Y. Sanbonmatsu, Magnesium fluctuations modulate RNA dynamics in the SAM-I riboswitch, J. Am. Chem. Soc. 134 (2012) 12043–12053.
[13] A. Yildirim, M. Sharma, B.M. Varner, L. Fang, M. Feig, Conformational preferences of DNA in reduced dielectric environments, J. Phys. Chem. B 118 (2014) 10874–10881.
[14] M. Sekijima, C. Motono, S. Yamasaki, K. Kaneko, Y. Akiyama, Molecular dynamics simulation of dimeric and monomeric forms of human prion protein: insight into dynamics and properties, Biophys. J. 85 (2003) 1176–1185.
[15] V. Gapsys, B.L. de Groot, R. Briones, Computational analysis of local membrane properties, J. Comput. Aided Mol. Des. 27 (2013) 845–858.
[16] H.I. Ingolfsson, M.N. Melo, F.J. van Eerden, C. Arnarez, C.A. Lopez, T.A. Wassenaar, X. Periole, A.H. de Vries, D.P. Tieleman, S.J. Marrink, Lipid organization of the plasma membrane, J. Am. Chem. Soc. 136 (2014) 14554–14559.
[17] Z.A. Levine, R.M. Venable, M.C. Watson, M.G. Lerner, J.E. Shea, R.W. Pastor, F.L.H. Brown, Determination of biomembrane bending moduli in fully atomistic simulations, J. Am. Chem. Soc. 136 (2014) 13582–13585.
[18] A.J. Sodt, M.L. Sandar, K. Gawrisch, R.W. Pastor, E. Lyman, The molecular structure of the liquid-ordered phase of lipid bilayers, J. Am. Chem. Soc. 136 (2014) 725–732.
[19] I. Buch, T. Giorgino, G. De Fabritiis, Complete reconstruction of an enzyme-inhibitor binding process by molecular dynamics simulations, Proc. Natl. Acad. Sci. U. S. A. 108 (2011) 10184–10189.
[20] P. Doruker, A.R. Atilgan, I. Bahar, Dynamics of proteins predicted by molecular dynamics simulations and analytical approaches: application to α-amylase inhibitor, Proteins: Struct. Funct. Bioinform. 40 (2000) 512–524.
[21] Y. Shan, et al., How does a drug molecule find its target binding site, J. Am. Chem. Soc. 133 (2011) 9181–9183.
[22] I. Bártová, et al., Activation and inhibition of cyclin-dependent kinase-2 by phosphorylation; a molecular dynamics study reveals the functional importance of the glycine-rich loop, Protein Sci. 13 (2004) 1449–1457.
[23] H. Alonso, A.A. Bliznyuk, J.E. Gready, Combining docking and molecular dynamic simulations in drug design, Med. Res. Rev. 26 (2006) 531–568.
[24] J.M. Adams, S. Cory, The Bcl-2 protein family: arbiters of cell survival, Science 281 (1998) 1322–1326.
[25] R.J. Youle, A. Strasser, The BCL-2 protein family: opposing activities that mediate cell death, Nat. Rev. Mol. Cell Biol. 9 (2008) 47–59.
[26] A. Ashkenazi, et al., From basic apoptosis discoveries to advanced selective BCL-2 family inhibitors, Nat. Rev. Drug Discov. 16 (2017) 273–284.
[27] F. Némati, et al., Targeting Bcl-2/Bcl-XL induces antitumor activity in uveal melanoma patient-derived xenografts, PLoS One 9 (2014) e80836.
[28] L. Bai, et al., BM-1197: a novel and specific Bcl-2/Bcl-xL inhibitor inducing complete and long-lasting tumor regression in vivo, PLoS One 9 (2014) e99404.

[29] J.D. Leverson, et al., Exploiting selective BCL-2 family inhibitors to dissect cell survival dependencies and define improved strategies for cancer therapy, Sci. Transl. Med. 7 (2015), 279ra40.

[30] G. Lessene, et al., Structure-guided design of a selective BCL-XL inhibitor, Nat. Chem. Biol. 9 (2013) 390–397.

[31] J.D. Leverson, et al., Potent and selective small-molecule MCL-1 inhibitors demonstrate on-target cancer cell killing activity as single agents and in combination with ABT-263 (navitoclax), Cell Death. Dis. 6 (2015) e1590.

[32] A. Kotschy, et al., The MCL1 inhibitor S63845 is tolerable and effective in diverse cancer models, Nature 538 (2016) 477–482.

[33] J.P. Hughes, et al., Principles of early drug discovery, Br. J. Pharmacol. 162 (2011) 1239–1249.

[34] D.J. Huggins, W. Sherman, B. Tidor, Rational approaches to improving selectivity in drug design, J. Med. Chem. 55 (2012) 1424–1444.

[35] N. Civjan, Chemical Biology: Approaches to Drug Discovery and Development to Targeting Disease, John Wiley & Sons, 2012.

[36] C. Tse, et al., ABT-263: a potent and orally bioavailable Bcl-2 family inhibitor, Cancer Res. 68 (2008) 3421–3428.

[37] W.H. Wilson, et al., Navitoclax, a targeted high-affinity inhibitor of BCL-2, in lymphoid malignancies: a phase 1 dose-escalation study of safety pharmacokinetics, pharmacodynamics, and antitumour activity, Lancet Oncol. 11 (2010) 1149–1159.

[38] A.W. Roberts, et al., Substantial susceptibility of chronic lymphocytic leukemia to BCL2 inhibition: results of a phase I study of navitoclax in patients with relapsed or refractory disease, J. Clin. Oncol. 30 (2011) 488–496.

[39] H. Zhang, et al., Bcl-2 family proteins are essential for platelet survival, Cell Death Differ. 14 (2007) 943–951.

[40] K.D. Mason, et al., Programmed anuclear cell death delimits platelet life span, Cell 128 (2007) 1173–1186.

[41] A.J. Souers, et al., ABT-199 a potent and selective BCL-2 inhibitor, achieves antitumor activity while sparing platelets, Nat. Med. 19 (2013) 202–208.

[42] Z.F. Tao, et al., Discovery of a potent and selective BCL-XL inhibitor with *in vivo* activity, ACS Med. Chem. Lett. 5 (2014) 1088–1093.

[43] T. Oltersdorf, et al., An inhibitor of Bcl-2 family proteins induces regression of solid tumours, Nature 435 (2005) 677–681.

[44] E.F. Lee, et al., Crystal structure of ABT-737 complexed with Bcl-xL: implications for selectivity of antagonists of the Bcl-2 family, Cell Death Differ. 14 (2007) 1711–1713.

[45] M.F.T. Koehler, et al., Structure-guided rescaffolding of selective antagonists of BCL-XL, ACS Med. Chem. Lett. 5 (2014) 662–667.

[46] H.M. Berman, et al., The protein data bank, Nucleic Acids Res. 28 (2000) 235–242.

[47] C. Shelley John, et al., Epik: a software program for pKa prediction and protonation state generation for drug-like molecules, J. Comput.-Aided Mol. Des. 21 (12) (2007) 681–691.

[48] Li Hui, D. Andrew Robertson, H. Jan Jensen, Very fast empirical prediction and rationalization of protein pKa values, Proteins: Struct. Funct. Bioinform. 61 (4) (2005) 704–721.

[49] E. Harder, et al., OPLS3: a force field providing broad coverage of drug-like small molecules and proteins, J. Chem. Theory Comput. 12 (2015) 281–296.

[50] Schrödinger Release 2017-2. Desmond Molecular Dynamics System, D. E. Shaw Research, New York, NY, 2017. Maestro-Desmond Interoperability Tools, Schrödinger, New York, NY, 2017.

[51] M. Bergdorf, S. Baxter, C.A. Rendleman, D.E. Shaw, Desmond/GPU performance as of November 2016, DEShaw Research Technical Paper, DESRES/TR-2016-01, 2016. https://www.deshawresearch.com/publications/Desmond-GPU%20Performance%20as%20of%20November%202016.pdf.

[52] S. Nosé, A unified formulation of the constant temperature molecular dynamics methods, J. Chem. Phys. 81 (1984) 511–519.

[53] W.G. Hoover, Canonical dynamics: equilibrium phase-space distributions, Phys. Rev. A 31 (1985) 1695.

[54] G.J. Martyna, D.J. Tobias, M.L. Klein, Constant pressure molecular dynamics algorithms, J. Chem. Phys. 101 (1994) 4177–4189.

[55] C.Y. Yang, S. Wang, Hydrophobic binding hot spots of Bcl-xL protein- protein interfaces by cosolvent molecular dynamics simulation, ACS Med. Chem. Lett. 2 (2011) 280–284.

[56] S.W. Muchmore, et al., X-ray and NMR structure of human Bcl-xL: an inhibitor of programmed cell death, Nature 381 (1996) 335–341.

[57] A. Oberstein, P.D. Jeffrey, Y. Shi, Crystal structure of the Bcl-XL-Beclin 1 peptide complex Beclin 1 is a novel BH3-only protein, J. Biol. Chem. 282 (2007) 13123–13132.

[58] M. Sattler, et al., Structure of Bcl-x L-Bak peptide complex: recognition between regulators of apoptosis, Science 275 (1997) 983–986.

[59] V. Kanakaveti, et al., Importance of functional groups in predicting the activity of small molecule inhibitors for Bcl-2 and Bcl-xL, Chem. Biol. Drug Des. 90 (2017) 308–316.